EFDA–JET–PR(09)41

L. Barrera, E. de la Luna, L. Figini, M.N.A. Beurskens, M. Brix, F. Castejón, P.C. deVries, D. Farina, M. Kempenaars, P. Lomas, J Mailloux, I. Nunes, E. Solano and JET EFDA contributors

Inboard and Outboard Electron Temperature Pedestal Profiles at JET Measured with ECE Diagnostics

Inboard and Outboard Electron Temperature Pedestal Profiles at JET Measured with ECE Diagnostics

L. Barrera[1], E. de la Luna[1], L. Figini[2], M.N.A. Beurskens[3], M. Brix[3], F. Castejón[1], P.C. deVries[4], D. Farina[2], M. Kempenaars[3], P. Lomas[3], J Mailloux[3], I. Nunes[5], E. Solano[1] and JET EFDA contributors*

JET-EFDA, Culham Science Centre, OX14 3DB, Abingdon, UK

[1]Laboratorio National de Fusión por Confinamiento Magnético Asociación EURATOM-CIEMAT, Madrid, Spain
[2]Istituto di Fisica del Plasma CNR, EURATOM-ENEA CNR Association, Milano, Italy
[3]EURATOM-CCFE Fusion Association, Culham Science Centre, OX14 3DB, Abingdon, OXON, UK
[4]FOM Institute Rijnhuizen, EURATOM-Association, P.O. BOX 1207, 3430BE, Nieuwegein, Netherlands
[5]Centro de Fusao Nuclear, Associacao EURATOM-IST, Lisboa, Portugal
** See annex of F. Romanelli et al, "Overview of JET Results",*
(Proc. 22 [nd] IAEA Fusion Energy Conference, Geneva, Switzerland (2008)).

Preprint of Paper to be submitted for publication in
Plasma Physics and Controlled Fusion

ABSTRACT

In this paper a novel use of the heterodyne radiometer in JET is presented. The operation of the diagnostic has been extended to allow measuring simultaneously the pedestal temperature profile at the inboard and outboard midplane with high spatial and temporal resolution. The radiometer in JET consists of 96 closely spaced channels distributed in 4 bands that can be set up to measure either first harmonic ordinary mode or second harmonic extraordinary mode electron cyclotron emission. Access to the inboard midplane region is obtained by measuring the O-mode polarization (no harmonic overlap) using an antenna located on the low field side of the torus. To assess the potential of the ECE temperature measurements in the inboard pedestal region, a detailed analysis of ECE spectrum will be discussed. The measured electron temperature profile are presented along with the method employed to calibrate the fundamental O-mode emission, including a discussion of the main uncertainties in the analysis. The comparison of inboard and outboard temperature pedestal profiles in a variety of H-mode plasmas shows a reasonable agreement in both shape and magnitude. Plans for the further exploitation of this new experimental data are also discussed.

1. INTRODUCTION

The high confinement regime (H-mode) is characterized by the formation of a transport barrier near the plasma boundary. This barrier produces a radially localized region of steep gradients in the temperature (T_e) and density (n_e) profiles which extends over a small fraction of plasma minor radius near the separatrix (so called 'pedestal' region). The high pedestal pressure achieved in H-mode plasma leads to the development of MHD instabilities called edge localized modes (ELMs) that cause a fast ($\sim$100 μs) [1] and repetitive loss of energy and particles from the pedestal. Although the increased particle transport induced by the ELMs has the beneficial effect of providing a mechanism to control the electron and impurity content of the plasma in large fusion devices, ELMs have the disadvantage of the large heat and particle loads that can potentially damage the plasma facing components of the machine.

Studies of the H-mode transport barrier in JET and other tokamaks (see [2] and references therein) have shown that the edge pedestal parameters play a crucial role in determining the global confinement quality of the core plasma. Thus, it is not surprising that a considerable theoretical and experimental effort has been devoted in the past decades to its study. Despite those efforts, the present understanding of the H-mode physics is far from being complete and there are still large uncertainties in extrapolating H-mode operation from present day devices to future burning plasma machines like ITER [2]. Part of the ongoing difficulty in determining the relevant physics is that the investigation of the pedestal region requires high spatial and temporal resolution measurements: parameters can vary by an order of magnitude over a few centimetres and on sub-milliseconds timescales. Much of the effort

of the fusion community on this topic has been devoted to measuring the fast evolution of the edge plasma parameters during the ELMing H-mode phase on the outboard midplane. More challenging is the experimental investigation of the behaviour of the inboard pedestal profiles and, typically, poloidal symmetry in electron density and temperature is assumed. The difficulty of access to the inboard region of the vacuum vessel makes, in general, very problematic the implementation of any diagnostics in this region and very few examples can be found in the literature. Fast measurements of the density profile on the inboard/outboard region in ASDEX-U have been obtained with reflectometry in ASDEX-U [3] and a Thomson Scattering system installed in MAST is capable of providing simultaneous measurements of the inboard and outboard density and temperature profiles [4]. In ASDEX-U the width of the density pedestal profiles on both regions is very similar in flux coordinates, while in MAST the pedestal density width is similar in radial space but not in the normalized flux coordinates.

In JET (R=2.96 m, a=0.95 m, with R the major radius and a the minor radius), the main diagnostics employed for the analysis of the temperature profile in the pedestal region are a High Resolution Thomson Scattering system (HRTS, using a 20 Hz, 5J, Nd:YAG laser) [5] that measures the T_e and n_e profiles on the outer midplane of the plasma (R=2.9-3.9 m), with a spatial resolution of $\sim$2 cm (with a channel separation of $\sim$1.5 cm) and a 96 channels heterodyne radiometer [6] which combines good spatial ($\sim$1-2 cm in the pedestal region, depending on plasma parameters) and temporal resolution (5 kHz with the standard acquisition system and up to 1 MHz for fast measurements). These systems give complementary information. The high temporal resolution of the radiometer is very useful to follow the fast dynamics of the pedestal temperature during the ELM cycle, whereas the better spatial resolution of the HRTS allows determining the electron density and temperature pedestal width with higher accuracy. In addition to these diagnostics, the temperature profile is also measured by the LIDAR Thomson Scattering system[7] with a nominal spatial resolution of $\sim$12 cm (4 Hz laser pulse repetition rate) which also provides the electron density in the core.

The aim of this paper is to examine new methods of improving the characterization of the edge pedestal region in JET. For this purpose, the operation of the heterodyne radiometer in this device has been extended to provide simultaneous measurements of the temperature profile in the pedestal region at the inboard and outboard midplane. The access to the inboard region is achieved by measuring fundamental harmonic Ordinary mode (denoted by 1O-mode) electron cyclotron emission (ECE) using an antenna located on the low field side of the machine. Since the optical depth of the second harmonic eXtraordinary mode emission (denoted by 2X-mode) is higher for a given plasma condition than that of the 1O-mode, standard T_e diagnostics based on ECE measurements typically employ 2X-mode data. However, in small aspect ratio tokamaks such as JET ($R/a \sim$3), the second harmonic emission from the inboard side of the plasma axis (from $R \leq$ 2.6 m in the case of JET, see figure 1) occurs at the same frequency as the third harmonic emission from near the outboard

plasma edge, preventing the use of 2X-mode emission to obtain local T_e measurements close to the inboard midplane. In view of these limitations, we decided to explore the use of the fundamental O-mode emission. For the typical plasma parameters obtained in the JET pedestal region, the optical thickness of the 1O-mode emission is sufficiently high to provide local T_e measurements and has the additional advantage of not being restricted by harmonic overlap. To the knowledge of the authors this is the first time that high resolution profile data have been obtained in the inboard region using this method.

Given the relative novelty of the technique, this paper focuses on the validation of the new inboard profile data, and the identification of the limitations of the measurements and the data analysis. The paper is organized as follows. The characteristics of the ECE diagnostics available in JET are briefly described in section 2. In section 3, simulated ECE spectra, for both O-mode and X-mode, are analyzed for typical JET H-mode plasma parameters and compared with measured data. This serves to illustrate the potential of the first harmonic O-mode ECE data to provide local temperature measurements on the inboard pedestal region in terms of spatial resolution, accuracy and limitations in its applicability. These topics together with the calibration techniques employed to obtain temperature from the fundamental harmonic O-mode ECE data are discussed in section 4. Few examples of the inboard and outboard pedestal electron temperature profiles measured by ECE radiometer are presented in section 5 to illustrate the capabilities of the diagnostic, together with a description of the analysis technique adopted for the comparison of these two set of measurements. Section 6 contains a summary and a discussion of the results.

2. ECE DIAGNOSTICS IN JET

The ECE spectrum in JET is measured using two instruments: a Michelson interferometer and a 96 channels heterodyne radiometer. Both diagnostics view the plasma normal to the magnetic field along horizontal sight lines near the plasma midplane, using antennas (open waveguides with dimension 50×65 mm) located on the outboard side of the tokamak. The two instruments observe the plasma with slightly different lines of sight. The radiometer antenna is located at z=0.133 m, while the antenna of Michelson interferometer is at z=0.353 m. The magnetic axis typically lies at z ∼0.26 m in JET, slightly closer to the Michelson line of sight. A wire grid polarizer just before each instrument is used to pass either the vertically or horizontally polarized emission which corresponds approximately to the X- and O-mode (quasi X- and quasi O-mode) respectively. In JET, the thermal plasma is always optically thick for both 1O-mode and 2X-mode emission (typically for T_e >0.3 keV) and this part of the spectrum is used to measure the T_e profile. The Michelson interferometer measures the emission in X-mode in the range of 70-350 GHz (covering several ECE harmonics) with an average frequency resolution of ∼10 GHz, typically corresponding to a spatial resolution of ∼15 cm for the second harmonic, and temporal resolution

of $\sim$15 ms. The instrument is absolutely calibrated. The uncertainty in the absolute calibration is estimated to be $\sim$10% and the relative systematic errors (estimated from the frequency variation of assumed-to-be smooth spectra) are of the order of $\sim$5%. The JET heterodyne radiometer is one of the most complete systems of this type. The original design includes 6 independent heterodyne receivers, covering a frequency range between 69-139 GHz. Each receiver can be set up to measure O- or X-mode radiation (for first or second harmonic respectively). This arrangement was chosen to accommodate the flexibility of JET to operate in a large range of toroidal fields and allows measuring the T_e profile for 1.65 T$\leq$ B_0 $\leq$4 T. Typically the 2X-mode ECE was used for low magnetic field plasmas and the 1O-mode for the higher magnetic fields. In 2008 the radiometer was upgraded by adding 6 new high frequency receivers, increasing the upper frequency limit up to 207 GHz, which allows the use of second harmonic X-mode also for B_0 $\geq$2.4 T. In each pulse, between 4 and 6 of the 12 available receivers are selected (depending on the magnetic field) in order to get the best profile coverage with 96 closely spaced channels ($\sim$1 cm channel separation, depending on the magnetic field gradient) with 250 MHz bandwidth. The radiometer data is cross-calibrated against the absolutely calibrated Michelson interferometer during the ohmic phase of the discharge.

The better spatial resolution (see section 4) and the higher cut-off density make the 2X-mode the preferred option for temperature profile measurements using ECE diagnostics. The interest of measuring 1O-mode emission lies mainly on the fact that it allows the access to the edge pedestal region on the inboard midplane otherwise inaccessible by the 2X-mode emission due to the harmonic overlap. In the case of the JET radiometer, it is possible to measure simultaneously the temperature profile in the pedestal region at both inboard and outboard midplane by using a combined 1O and 2X-mode operation. This mode of operation is available in JET only for a subset of toroidal magnetic field: B_0=2.4 T, 2.7 T, 3.0 T. This is illustrated in figure 1 where the 2X and 1O-mode resonant frequencies as function of the major radius are shown together with the T_e profiles measured by the LIDAR Thomson Scattering diagnostic and the ECE radiometer for a JET discharge with B_0=2.4 T. The radiometer uses two receivers (48 channels) to measure the 1O-mode in the inboard midplane and two receivers to measure the 2X-mode in the outboard region. Since each of these diagnostics provide local T_e measurements at different poloidal locations, to compare the different T_e profile data, toroidal symmetry is assumed and measurements are mapped along surfaces of constant magnetic flux onto the midplane. The mapping is obtained from the magnetic EFIT equilibrium reconstruction [8]. In the remainder of the text we will refer to the inboard and outboard midplane as the High-Field-Side (HFS) and the Low-Field-Side (LFS) regions respectively.

3. ECE SPECTRA SIMULATIONS

A detailed analysis of the ECE spectrum for both X and O-mode has been carried out to assess the potential of the O-mode ECE to provide local T_e measurements in the edge region on the

HFS. The primary tool employed in our analysis is the SPECE code[9]. This is a ray tracing code, in which emission and absorption are computed solving the fully relativistic dispersion relation for EC waves, and accounts for multiple harmonic resonance. The effect of reflection at the walls is included by means of empirical coefficients for reflection (R_w) and polarization scrambling (R_p) due to wall reflections. In the simulations reported here we have used R_w=0.55 and R_p=0.38, which were adjusted for a best fit to the optically thin region of the measured spectra. The optical thickness (τ) is related to the plasma absorption and evaluated by direct integration of the absorption coefficient along the ray trajectory. The procedure to simulate a measured ECE spectrum is as follows. First a magnetic equilibrium is generated from magnetic probe data using the EFIT equilibrium code for the pulse and time of interest. This provides the magnetic flux coordinate and the total magnetic field geometry, including the vacuum magnetic field, the poloidal magnetic field generated by the plasma current and diamagnetic and paramagnetic corrections due to the plasma pressure gradient and the plasma azimutal current respectively. Next, the measured electron temperature profile either from the HRTS or ECE and the electron density profiles, from the HRTS or the deconvolution of several line integrated interferometer channels [10], are mapped onto the horizontal midplane (assuming all plasma parameters to be function of the flux coordinate) and fitted using cubic spline curves. Particular attention is paid to the profiles at the plasma edge where a hyperbolic tangent function [11] is used to fit the available experimental data in the pedestal edge region.

With these data the ECE spectrum in the X and O-mode and the quasi X and quasi O-mode (corresponding to ECE radiation with vertical and horizontal polarization respectively) as could be observed from the low-field side along the lines of sight of each instrument is calculated by the SPECE code. In this analysis the electron distribution function is assumed to be locally Maxwellian. A realistic viewing geometry of the different ECE instruments available in JET is also taken into account by means of a multi-ray calculation that includes a description of the antenna pattern. To finally obtain the T_e profile an additional step is required in order to assign a radial position to each frequency of the ECE spectrum in the region of interest for T_e measurements. As a first approximation, it is possible to assign the value of the radiation temperature to the radial position corresponding to the cold resonance location of the emitting frequency, R_{cold}, defined for a given frequency by $\omega = s\omega_{ec}(R_{cold}) = seB(R_{cold})/m_e$, where s is the harmonic number, B is the total magnetic field and e and m_e are the electron charge and rest mass, respectively. However, a more detailed analysis of the ECE localization must take into account the effect of the relativistic broadening. For observation perpendicular to the magnetic field, this broadening causes a down-shift in frequency of the emitted radiation, i.e., at a given frequency, the observed emission comes from a thin layer radially shifted inward with respect to the cold resonance position. Therefore, in addition to the total emitted intensity the code calculates, for each frequency, the average position from which the observed emission originates (R_{mean}) and the radial region, mapped onto the magnetic axis, contributing to the 95% of the emitted

radiation ($\Delta R_{95\%}$) that is used to quantify the spatial resolution of the measurements[12]. The spatial resolution is calculated considering the width of the emission layer, that depends on the optical depth, the mode number and polarization, and the antenna pattern in both poloidal and toroidal directions. The maximum density at which reliable temperature can be obtained by ECE diangostics is limited by cut-off, and for high-density plasmas, in cases where $\omega_p^2/\omega_{ce}^2 \rightarrow 1$ (where ω_p is the plasma frequency), the refraction experienced by the emitted radiation before arriving to the antenna (calculated by the ray tracing code) adds an additional radial shift to the ECE channels location. The 1O-mode emission frequency is closer to its cut-off frequency than the 2X-mode and therefore it is more susceptible to cut-off and refraction effects.

Figure 2(a) shows the comparison of the measured (symbols) and simulated (solid line) quasi X-mode ECE spectrum for the Michelson interferometer for a high density H-mode plasma (JET pulse:74220, B_0=2.7 T, I_p=1.8 MA, $n_{e,0}$=5$\times 10^{19} m^{-3}$, P_{NBI}=20 MW, P_{ICRH}=2 MW). To display the sensitivity of the calculations to the input parameters, the spectrum calculated by including errors on the input parameters ($\pm 10\%$ in T_e and n_e profiles) is also shown (dashed lines). In these plasma conditions, the second and third harmonic emission are optically thick and therefore they are mainly sensitive to changes in the temperature profile. The first thing to notice is that, although the magnitud of the second and third harmonic emission maxima is well reproduced by the simulation, there is a clear frequency shift between the measured and simulated spectrum that is outside the uncertainties on the input profiles. The frequency corresponding to the second and third harmonic emission peaks can only be correctly fit by applying a correction to the magnetic field. This is done in the SPECE code by rescaling the toroidal magnetic field as: $B_{t,new}^2 = B_t^2 + (k_{vac}^2 - 1)(R_0 \times B_0/R)^2$ where B_t is the uncorrected toroidal magnetic field, R_0=2.96 m, B_0 is the magnetic field value in vacuum at R_0, and k_{vac} is the ratio between the corrected and the measured vacuum magnetic field in JET, while keeping the topology of the flux surfaces unvaried. The simulation code is then run using different k_{vac} values until the best fit to the measured spectrum is found. The result of this analysis for the example mentioned above is shown in figure 2(b) where the simulated quasi X-mode spectrum for the radiometer line of sight including a magnetic field correction of 3% is compared with the spectrum measured by the Michelson interferometer. In this particular example, the magnetic axis is located at z=0.262 m, almost equidistant from the line of sight of the Michelson and the radiometer and no significant difference is observed between the peak temperatures measured by both diagnostics. The simulated quasi O-mode spectrum is also included in the figure. There is a remarkable good agreement between the measured and calculated spectra, even in the region below 100 GHz, which corresponds to O-mode emission that has suffered some polarization scrambling after being reflected back and forth between the vessel walls and the cut-off layer. The difference between the level of measured and calculated second harmonic emission at the plasma edge on the LFS (100$\leq$ F $\leq$125 GHz) is simply due to the higher frequency resolution used in the simulation. This good agreement gives us an added degree of confidence in the accuracy of the absolute calibration of the Michelson interferometer.

The frequency shift between the measured and computed ECE spectra shown in figure 2(a) is observed systematically in JET pulses and results in the appearance of a radial shift between the T_e profiles measured by HRTS and ECE diagnostics, with the ECE T_e profiles always shifted inwards with respect to the HRTS T_e profiles. The existence of an error in the location of the ECE T_e profiles is confirmed by the observation of very similar radial shifts between the location of the MHD islands obtained from fast ECE data and from charge exchange spectroscopy [13]. Note that including the correction in the mapping of the ECE measurements (typically $\Delta R_{rad} = R_{mean} - R_{cold} < 1$ cm in the outboard side of the plasma) would shift the T_e profile measured by ECE further inside and therefore it cannot explain this discrepancy. It is worth mentioning that, in spite of this discrepancy, the magnitude and overall shape of the T_e profiles derived from ECE (2X-mode) are generally in good agreement with those measured by Thomson Scattering. Discrepancies in the core temperature values measured by ECE and HRTS have been reported in JET in high temperature plasmas with predominant ion cyclotron resonant heating [14] but those are not included in this study. The error in the location of the T_e profiles measured by the ECE diagnostics arise from a variety of sources. In the case of L-mode plasmas the radial shift in the T_e profile measured by ECE can be corrected by simply including an error of $<1\%$ in the vacuum magnetic field, which is well within the uncertainty of its calibration. However, for H-mode plasmas (typically with higher β values and therefore with larger Shafranov shift) the radial shift is not uniform, varying from typically $\sim$5 cm in the LFS pedestal region to $\sim$10 cm in the plasma core, which indicates an additional source of error probably related to an inaccurate mapping of the magnetic axis by EFIT. The latter conclusion is perhaps not too surprising, given that the magnetic reconstruction uses rather simplified functions for the current and pressure profile as the input data for the solution of the Grad-Shafranov equation which tends to underestimate the Shafranov shift. It is worth noting that the magnetic field correction required to match the temperature profiles measured by HRTS and ECE in the pedestal region are typically $<1\%$ (generally the same correction used to match the whole T_e profile in L-mode regime). Higher magnetic field correction values are needed to match the ECE and the HRTS profiles in the core region; this discrepancy is also consistent with the higher magnetic field correction values required to match the frequency of the second and third harmonic peaks in the ECE spectra ($\sim 3\%$ for the example shown in figure 2). The source of these errors in the mapping of the ECE measurements is under investigation. However, since this paper is focused on the study of the pedestal profiles, in the following analysis the magnetic field correction has been adjusted to best match the ECE and the HRTS edge temperature profiles in the LFS region.

4. PEDESTAL T_E MEASUREMENTS USING 2X-MODE AND 1O-MODE ECE

We can now go back and examine the ECE simulated spectra shown in figure 2 in more detail, focusing our attention on the spectral range, for both 2X-mode and 1O-mode, used for temperature

profile measurements in the pedestal region. As mentioned previously, for typical JET plasma conditions, the use of the first harmonic O-mode allows measuring both the LFS and HFS of the plasma column, while with the 2X-mode the pedestal region on the HFS is not accessible because of the overlap between the second and the third harmonic.

Figure 3(a) compares the pedestal temperature profiles derived from the 2X-mode (LFS) and the 1O-mode (HFS) ECE simulated spectra to the profile which was used as input for the simulation shown in 2 (pulse 74220 with $n_{e,ped}$ = 3×10^{19} m^{-3} and $T_{e,ped}$ = 2 keV). The HFS temperature profile is mapped to the outer midplane and overlaid with the LFS temperature profile and the results of the mapping using both ρ_{cold} and ρ_{mean} are shown in the figure, where ρ is the normalized minor radius. For comparison a second simulation using the parameters of a pulse with higher density $n_{e,ped}$ = 6.5×10^{19} m^{-3} and lower temperature $T_{e,ped}$ = 0.8 keV is also included. In both cases, the mapping includes a magnetic field correction factor of 0.8%. As discussed in the previous section this correction is needed to bring into alignment the HRTS and the LFS ECE T_e profiles in the pedestal region. These two pulses have been chosen to illustrate the impact of the optical depth on the ECE measurements. In this example, an increase in the pedestal density (and hence in the optical depth) by almost a factor of two implies an increase in spatial resolution of a similar value (this will be discussed in more detail in section 4.3) which will have important consequences on the level of accuracy of the temperature measurements that can be obtained from the ECE data.

We begin the discussion by considering what happens when we apply the usual simple analysis of using the cold resonant condition to locate the observed emission at each frequency. In this case, two observations about the profiles shown in figure 3 can be made: a radial shift appears between the input data and the deduced profile when the ρ_{cold} coordinates are used and an overestimate of the T_e or 'enhanced radiation' is observed in the LFS edge region. The shift between the input and calculated profile can be understood by considering that, as a consequence of the relativistic broadening of the emitted radiation, the location of the emission will move towards a higher magnetic field region. For the usual case of decreasing temperature towards the edge, this results in a profile that will be shifted outwards in the LFS region and inwards in the HFS region. As shown in figure 3, this effect can be properly corrected by calculating the T_e profile using ρ_{mean} instead of ρ_{cold}. Typical values of the relativistic correction ($R_{mean} - R_{cold}$) for H-mode JET plasmas range from 0.5 to 1 cm in the LFS pedestal region and from 1 to 1.5 cm in the HFS pedestal region. The radial shift increases with decreasing optical depth and consequently it is larger for the lower density case. The lower optical depth of the 1O-emission also causes a larger shift on the HFS profiles than in the LFS profiles. The relative error $\Delta T_{rad} = (T_e(R) - T_{rad}(R))/T_e(R)$ in the HFS region at the pedestal top for the profile using ρ_{cold} can reach values up to $\sim 15\%$ in low density plasmas, although the overall shape of the profile is very similar to the input profile.

To asses quantitatively the utilization of the first harmonic O-mode for edge pedestal temperature

measurements on the HFS, this section will examine four important aspects of the ECE measurements: 1) the calibration method employed to calculate the temperature from the 1O-mode emission data, 2) the observed 'enhanced radiation' in the LFS edge region, 3) the spatial resolution of the observed emission in the first harmonic O-mode and second harmonic X-mode frequency range and 4) the overall accuracy of the ECE T_e pedestal measurements.

4.1. CALIBRATION OF FIRST HARMONIC ORDINARY MODE RADIOMETER CHANNELS

In JET, the standard calibration of the ECE radiometer data is provided by a Michelson interferometer measuring the second X-mode ECE which is absolutely calibrated. Since this method is not longer possible for the first harmonic O-mode emission at frequencies resonating on the HFS region, two independent calibration methods were developed. The first method is based on the measurement of the first harmonic O-mode ECE for a certain frequency at two different times of a discharge having significantly different magnetic field. The magnetic field at the calibration time must be high enough so that the radiometer channels measuring first harmonic with frequencies that resonate in the HFS pedestal region at the beginning of the pulse reach the region where the second harmonic emission is free from harmonic overlap (3.7 m$>$ R $>$2.6 m, see figure 1). By using specific toroidal field ramp pulses it is possible to cross-calibrate the O-mode channels against the Michelson interferometer, assuming that O and X-mode emission does not differ significantly. A very good agreement is found between both radiometer (1O) and interferometer (2X) spectra when both lines of sigh are equidistant to the plasma equatorial plane and when both harmonics are optically thick (for sufficiently high density and temperature). In these conditions, the only difference between the radiation temperatures measured by the two polarizations is attributable to their different spatial resolution (better for 2X-mode due to its higher optical depth).

The calibration pulse was not available for every JET experiment in which the HFS/1O-mode ECE data were collected and the variability of the measured calibration factors (mainly due to lack of stability on the receiver's sensitivity) made necessary to develop an alternative calibration technique. The second method uses the simulated spectra to cross-calibrate the radiometer 1O-mode ECE channels, adjusting the magnetic field until the simulated and measured 2X-mode radiation temperature are in agreement. In order to obtain a reliable calibration the following conditions must be fulfilled: the method is restricted to L-mode plasmas, where uncertainties in the equilibrium reconstruction are assumed to be smaller, and the calibration radial region is restricted to 0.3 $<$ ρ $<$ 0.8. Here the lower limit is chosen to guarantee high enough optical thickness (with T_e $>$300 eV) and the upper limit is imposed to avoid fast temperature variations due to MHD activity (sawteeth) in the plasma core. The error in the calibration is calculated by comparing the calibration factors obtained using the second method in cases where the absolute calibration is available. This comparison gives an error of $\leq$10$\%$ which gives us confidence in the calibration procedure.

4.2. ECE MEASUREMENTS CLOSE TO THE SEPARATRIX

Closer inspection of the ECE spectra shown in figure 2 reveals a characteristic feature in the low frequency spectral region that, as mentioned previously, has important consequences for the pedestal temperature measurements. Strong peaks appear at low frequencies for both the 2X-mode (110$\leq F \leq$ 125 GHz) and the 1O-mode (60$\leq F \leq$ 70 GHz). This is a well-known ECE feature that appears systematically in the edge region of H-mode plasmas correlated with the appearance of steep gradients in density and temperature profiles [15, 16]. This is more clearly seen in figure 4 where the radiation temperature profile measured by the ECE radiometer (2X-mode) together with the simulated profile for the same pulse of figure 2 are shown. The figure shows the ECE channels mapped onto the midplane considering ρ_{cold} and ρ_{mean}. The profile derived from the simulated data is plotted versus ρ_{cold}. When using ρ_{cold} to map the ECE channels, the radiation temperature measured by ECE for $\rho >$0.98 appears to be higher than the T_e (derived from HRTS measurements) and a local maximum appears outside the last close flux surface (the separatrix). This effect is well reproduced by the simulation and can be attributed to relativistically downshifted thermal emission located at smaller radii that is not fully reabsorbed due to insufficient optical depth at the plasma edge [17]. To interpret this result one has to remember the fact that, since the EC frequency depends on both the local magnetic field along the line of sight and the energy of the resonant electrons, the emission at a given frequency is originated by electrons of different energies, with the energy of the resonant electrons (for perpendicular observation $E = mc^2(s\omega_{ce}/\omega - 1)$) increasing with the difference between the local cyclotron frequency and the observation frequency (ω). In H-mode plasmas, the high T_e in the pedestal region implies that a relatively large number of high energy electrons in the tail of the Maxwellian exists few centimetres inside the separatrix. Due to the low density and temperature (and hence optical depth) at the plasma edge there is some emission generated by these high energy electrons that can escape the plasma without substantial reabsorption. As a consequence, the region from which the measured radiation is originated broadens (indicated by the horizontal bars in figure 3) and there is an inward shift of the effective measurement position that is very large for the ECE channels whose cold resonance location is in the optically thin region for $\rho >$0.98 (represented by open symbols in figure 4). At even larger radii, which correspond to lower observation frequencies, the observed intensity decreases because the required resonant energy is too high and the number of high energy electrons that can contribute to the emission falls rapidly. For perpendicular observation, the downshifted emission originates in the region located on the high field side of the cold resonance position. Therefore, this leads to the appearance of a region of 'enhanced radiation' close to the separatrix on the LFS (for both 1O and 2X-mode) but not on the HFS (for 1O-mode). In fact, this feature establishes a constraint on the minimum electron temperature for which the ECE measurements can provide reliable temperature measurements in the LFS.

4.3. SPATIAL RESOLUTION OF SECOND HARMONIC X-MODE AND FIRST HARMONIC O-MODE ECE MEASUREMENTS

An important aspect to consider when evaluating the potential of using ECE diagnostics to measure the electron temperature profile is the degree of radial localization of the emission. As described in section 3, at each frequency, the measured radiation intensity is the integral over a finite spatial region and the width of the region from which 95% of the observed emission originates is the criteria used to quantify the spatial resolution of the measurements. Extensive use of the SPECE code has been made to asses the radiometer achievable spatial resolution in the pedestal region, for both the 2X and 1O-mode emission. The effects considered in this calculation are: the spatial resolution transverse to the line-of-sight of the radiometer that is determined by the difraction pattern of the receiving optics and the relativistic broadening of the emission that depends on the optical depth. The antenna pattern was simulated using a Gaussian profile with a beam waist of 2 cm which is consistent with the diffraction pattern of the radiometer antenna. Since the optical depth depends on the density and temperature profile, the magnetic field gradient, the harmonic number and the polarization mode, the spatial resolution must be computed for each radiometer channel and each individual profile.

An example of this study is shown in figure 5 where the spatial resolution ($\Delta R_{95\%}$) for typical JET H-mode plasma parameters is depicted versus the mean radial location of the observed emission (R_{mean}), mapped onto the midplane, for frequencies resonanting on the HFS (1O-mode) and the LFS (2X-mode) regions. The separatrix on the inboard and outbard midplane is located at $\sim$1.98 m and $\sim$3.85 m, respectively. In this case we have used the simulation code to explore the dependence of the computed spatial resolution on changes on the electron density and temperature. Simulations are performed using the global parameters of the pulse 73340 (B = 2.7 T, I_p=2.5 MA, P_{NBI}=14 MW) and two more cases have been calculated by rescaling independently the density and temperature profiles of the reference pulse. The parameters used in these simulations are listed in Table I and can be considered representative of the database analyzed in this paper. The results of the the single-ray and multi-rays calculations, i.e. taking into account the antenna pattern, are included in the figure. Note that in the case of a single ray calculation, when approaching the plasma centre the ray becomes tangent to the flux surfaces (the line of sight of the radiometer has typically a vertical offset $\sim$10-15 cm with respect to the horizontal midplane) and the width of the emission layer (once mapped onto the midplane) becomes 'artificially' very small.

As it can be seen in the figure 5, the major contribution to the radial resolution near the edge comes from the intrinsic width of the emitting layer (single ray), whereas the resolution tends to become worse at the plasma centre, where the dominant effect is the divergence of the beam. The intrinsic spatial resolution for the 2X-mode is almost half than that of the 1O-mode because of its higher optical thickness. Its value decreases with increasing density and decreasing temperature, for fixed

Table 1: Profile parameters used in the simulations shown in figure 4

Case	n_e (10^{19} m^{-3})		T_e (keV)	
	Core	Pedestal	Core	Pedestal
A	8	6.5	4.6	1.1
B	5	3.5	4.6	1.1
C	5	3.5	8.4	2.0

magnetic field gradient and observing angle [17]. The lower frequencies and the longer distances from the emitting region to the antenna located on the outboard side of the tokamak make the contribution of the antenna pattern to the effective radial resolution larger for the 1O-mode/HFS than for the 2X-mode/LFS data, rising the effective resolution on the HFS above the intrinsic line emission width by 1 to 2 cm. As shown in the figure this effect is more pronounced at higher densities due to the stronger refraction experienced by that beam as the cut-off density is approached. Thus the situation is worse for low magnetic fields and/or higher densities.

From our analysis we conclude that the ECE measurements are well localized in the pedestal region in low to moderate density plasmas, with the effective spatial resolution for the 1O-mode on the HFS being approximately twice than that of the 2X-mode at the LFS. In those conditions, the estimated spatial resolution varies between 1 to 2 cm (depending on the local plasma parameters) at the LFS (2X-mode) and between 3 to 5 cm on the HFS (1O-mode). Since the flux expansion is larger in the inboard region, the spatial resolution in normalized flux co-ordinates is comparable on both regions, although small differences in the measured gradient could be expected. These values should be considered as a lower limit since they do not include the finite instrumental bandwidth of the diagnostic (its contribution being very small in the case of the radiometer, $\Delta R_{filter} = \frac{\partial R_{50\%}}{\partial f} \times \Delta f_{filter}$ <0.5 cm with Δf_{filter}=250 MHz) and only a simple diffraction model has been used to simulate the antenna pattern. It is worth mentioning that the resolution of the JET radiometer data in the outboard pedestal region is comparable to that of the HRTS ($\sim$ 2 cm). In order to use the 1O-mode emission to access the inboard midplane region the density should be sufficiently below the cut-off density (typically $n_e/n_{e,cut-off} < 3/4$) to avoid too strong refraction of the rays and a deterioration of the spatial resolution.

Finally, the question of how much smoothing is introduced in the measured profiles due to the finite spatial resolution has to be addressed. This is particularly important for the analysis of pedestal region in H-mode plasmas, where the width of the pedestal can be comparable to the spatial resolution of the measurements. In the case of JET, the pedestal width of the electron temperature profile in H-mode plasmas typically is $\sim$ 3 cm [18], which corresponds to $\sim$ 5 cm at the inboard midplane due to the poloidal flux expansion. The effect of the radial resolution on the measured profiles can be modeled by performing a convolution of a step profile (with infinite gradient) with the instrumental kernel, which, for the case of the ECE radiometer channels, can be

computed by the SPECE code. The gradient of resulting convolved profile, that it is a smoothed version of the true profile, gives an idea of the maximum gradient that the diagnostic is able to measure. The pedestal width calculated by that method varies between 0.6 and 1.5 cm for the 2X-mode at the LFS and between 2.5 and 3.0 cm for the 1O-mode on the HFS for the same range of plasma parameters discussed above. Therefore, it is concluded from this analysis that the spatial resolution of both the 1O-mode (HFS) and 2X-mode (LFS) ECE measurements are acceptable although in both cases they are at the limit of the required resolution to fully resolve the gradients in the pedestal region.

4.4. CONSIDERATIONS OF ACCURACY OF THE ECE PEDESTAL T_E MEASUREMENTS

We can now compare the measured profiles with the results of the simulation. For the purpose of illustration the measured profile corresponding to the simulation depicted in figure 3(a) is shown in figure 6. For this comparison we have chosen to use the cold resonance position instead of ρ_{mean} to map the measured ECE profiles, which is the procedure routinely used in JET. The calculation of the shift due to the relativistic broadening of the emission for every pulse would require prohibitive amounts of computational time. Moreover, this shift is usually smaller (typically $\sim$1 cm and $\sim$1.5 cm for the LFS and the HFS pedestal region, respectively) than the one introduced by the uncertainty in the magnetic field ($\sim$5 cm in the LFS pedestal region). Using this criteria we find that the T_e profile inferred from the 2X-mode ECE data is in agreement with the simulated profiles at the LFS, but a radial outward shift between the 1O-mode ECE measured and simulated profiles is observed in the HFS region. This shift, which cannot be explained by calibration errors ($\leq 10\%$) alone, is larger for the pulses with low pedestal density (lower optical depth) as the one shown in figure 6. In spite of this discrepancy in the profile location, good agreement is observed, in shape and magnitude, between the profiles measured in both the HFS and the LFS regions. Although not shown here, the temperature values measured by ECE are generally consistent with the HRTS measurements. It has to be noted that the level of agreement obtained between the LFS and the HFS profiles is somewhat surprising since the choice we made in the mapping procedure (using ρ_{cold} instead of ρ_{mean}) should cause larger differences between the HFS and the LFS data (as it is deduced from the simulations). Two error sources have been identified that contribute to this result: a vacuum magnetic field calibration error and uncertainties in the equilibrium reconstruction described in section 3. One of the difficulties in this analysis is that the magnetic field error, as inferred from the comparison between HRTS and ECE profiles during the L-mode phase in a wide variety of discharges, is not a constant value, as one would expect from a purely calibration error. This is not completely understood at this time and intense work is in progress in this area. In general, a vacuum magnetic field correction factor between 0.2% and 0.8% is required to align the HRTS and the 2X-mode(LFS) ECE T_e profiles in H-mode plasmas, but this error is not enough to obtain a consistent comparison between simulated and measured

1O-mode(HFS) profiles. This indicates that, at least for the HFS data, an additional source of error on the equilibrium reconstruction needs to be invoked. On the one hand, the accuracy of the EFIT reconstruction to determine the position of the separatrix as well as the magnetic field in the pedestal region is limited since effects such the finite pressure gradient at the edge or the bootstrap current are not included. On the other hand the quality of the flux surfaces location inferred from EFIT is not necessarily the same on both regions (less magnetic probes are present on the inboard region). This is an important consideration since no independent diagnostic can be used to check the validity of the equilibrium reconstruction on the inboard region in JET. The situation is different in the LFS where the temperature profile from the HRTS can be used, within the uncertainty of the measurements, to cross-check the absolute position of the outboard separatrix determined from the EFIT reconstruction. A more detailed analysis of these and other sources of uncertainties in the mapping process is the subject of ongoing investigation. In principle, if one could remove the uncertainty in the magnetic field calibration, it would be possible to use the information provided by the 1O-mode ECE data as an additional constraint for the equilibrium reconstruction on the HFS region. This information together with the location of the magnetic axis, that can be easily determined from the measured ECE spectrum, could contribute to improve the magnetic equilibrium reconstruction in JET. This is a topic for future work.

5. COMPARISON OF LFS AND HFS T_E PROFILES IN THE PEDESTAL REGION

Systematic comparison of the simultaneous T_e profiles measurements on the HFS (1O-mode) and LFS (2X-mode) has been carried out for a wide range of plasma parameters. The edge operational space of the discharges chosen for this analysis is shown in figure 7(a). Here $T_{e,ped}$ and $n_{e,ped}$ are taken at the top of the pedestal from the HRTS measured profiles. The dataset includes pulses in advanced tokamak scenario at $q_{95} = 4.6$ (with B=2.7 T and I_p=1.8 MA), where q_{95} is the safety factor at 95% of the outermost flux surface, standard H-mode at q_{95}=3.3 and 3.6 (with 2.4 T/2.0 MA and 2.7 T/2.5 MA, respectively) and H-mode pulses obtained in the hot-ion plasma regime (2.7 T/2.5 MA)[19] which run at higher T_e than standard H-modes. As shown in the figure, the density covered in this analysis ranges from 2.5×10^{19} m^{-3} to 7×10^{19} m^{-3}, with the H-mode plasmas in advanced scenario having the lowest pedestal density and the highest pedestal temperature. All the pulses investigated here have an average triangularity δ_{av} varying from 0.36 to 0.42, are dominantly heated by NBI ($P_{NBI} \sim$ 10-22 MW) and have type I ELMs.

The comparison of the experimental data is done using the following procedure. Both LFS and HFS ECE profiles are mapped onto the midplane and a magnetic field correction factor is applied to force the consistency between the 2X-mode (LFS) ECE profiles and the HRTS profiles in the region around and inside the pedestal top. To reduce the scatter due to the ELMs in the results the so-called 'ELM-averaged technique' is used. During a time window (0.2-1 sec, depending on the

ELM frequency) where the plasma parameters are close to steady state conditions and the ELM size and period do not vary significantly, an averaged profile is built by grouping together data measured just before the ELM crash, mapped onto the midplane and then fitted as function of the normalized minor radius using the modified hyperbolic tangent function [11]. A time interval corresponding to $<20\%$ of the ELM cycle just before the ELM crash was considered in this analysis, with the onset time of the ELM taken from the D_α signal. In some cases a radial shift of $\sim$1 cm was applied to the HRTS profile to align the foot of the *mtanh* function with the plasma separatrix. This error is well within the accuracy at which the separatrix position in the midplane can be determined from magnetic probes in JET. With this adjustment, the fit values of the T_e at the separatrix are $\sim$100-150 eV. For the evaluation of the *mtanh* fit to the T_e profile in the LFS region the HRTS and ECE data are combined. In the case of the HFS data, an additional constraint on the T_e value ($<$150 eV) at the separatrix has been included. Similar procedures have been applied for the analysis of the measured pedestal profiles in other machines[20, 21]. An example of the results obtained from this type of analysis is presented in figure 7(b) showing the good agreement between the pedestal heights on the HFS inferred using the procedure describe above and those measured at the LFS.

To further illustrate the validity of the ECE measurements on the HFS region we have compared in figure 8 the T_e values measured by the radiometer on the HFS and the LFS at 5 different flux surfaces locations for ρ $>$0.7 for each pulse within the dataset shown in the figure 7(a). Those pulses where the refraction effects were noticeably affecting the location of the emission have not been included in this comparison. Only data points in the high optical thickness region ($\rho < 0.97$), as described in section 4, are included in the figure. We find a fair agreement between the T_e values measured at LFS and the HFS region, with the T_e values measured at the HFS profiles slightly lower ($\sim$ 7%) than those at the LFS as predicted by the ECE spectrum simulations discussed in section 4. This result is consistent with the assumption of the electron temperature to be poloidally constant on closed fluxed surfaces which is not surprising in view of the fast parallel electron heat flow. It should be noted that the difference between HFS and LFS temperature values is larger in the steep gradient region close to the separatrix. This is not surprising since it is in this region where the difference in spatial resolution between the HFS and LFS ECE data should be more noticeable. This causes the measured T_e profiles on the HFS to have slightly smaller gradients than that of the LFS.

A closer look to the profiles allows us to identify some of the relevant features in this comparison. Two examples of the temperature profiles measured by ECE and HRTS (when available) during a gas fuelling scan experiment in an advanced tokamak scenario with q_{95} = 4.6 (B_T =2.7 T, I_p =1.8 MA) and P_{NBI} = 18 MW)[22] are plotted in figure 9. In this experiment, almost no change is seen in the central line averaged density, with n_e/n_{GW}=0.52 (n_{GW} is the Greenwald density, I_p(MA)/[πa(m)^2] in units or 10^{20} m^{-3}) but the pedestal temperature decreases with increasing gas rate and, as a consequence, the confinement degrades with a reduction of $\sim$ 18% in stored

energy. During this scan both the LFS and the HFS profiles respond in a very similar way. The changes in pedestal pressure have a clear impact on the ELM characteristics, their size become smaller ($\Delta W_{ELM}/W_{MHD}$ varies from 13% to 3%) and their frequency increases from 12 Hz to 56 Hz. The result of the *mtanh* fits for the LFS T_e profiles are also shown in the figure. Within the accuracy of the measurements, the width of the pedestal temperature profiles appears to be similar in the LFS and HFS. As noted previously, the HFS pedestal width tends to be slightly higher than that of the LFS. As an example, the value of the temperature width in normalized minor radius coordinates for the profile in figure 9(b) is 0.048 for the LFS profile (combining ECE/2X-mode and HRTS data) and 0.056 for the HFS profile, which correspond to 3.8 cm and 7.5 cm in radial space, respectively. It is worth mentioning that since these values have been derived without taking into account the specific instrumental resolution of each diagnostic, they must be considered as the upper limits of the true pedestal width values. One more thing to mention is that the larger number of points in the HFS profile (smaller channel separation due to higher magnetic field gradient) does not increase the spatial resolution because at each point the emission is limited by the spatial resolution of the diagnostic.

The data shown in figure 9 highlights the difficulty of using ECE diagnostics to determine the electron temperature profile pedestal width. As described in section 4, the electron density and temperature and hence the optical thickness decreases significantly in the edge region making reliable local T_e measurements impossible in the vicinity of the separatrix. This means that radiation temperature measured for $\rho >$0.98 must be excluded from the temperature profile evaluation. In these conditions, the pedestal top temperature value can be reasonably derived from the ECE measurements, whereas the pedestal width, that depends sensitively on the temperature at the separatrix, cannot be determined with sufficient accuracy unless additional constraints are included. Moreover, the uncertainty in the profile location (see section 3) introduces an additional uncertainty in the determination of the pedestal width, up to +/-1 cm depending on the magnetic field correction factor. It is worth noting that, since both the magnetic field gradient and the poloidal flux expansion are smaller in the outer midplane, the relative error in the pedestal width is larger for the LFS than for the HFS profiles. Taking into account the uncertainties in this analysis we have not attempted yet to draw any firm conclusions on the comparison between the pedestal width on the HFS and the LFS and this work is left for future publications.

Another example of the measured ECE temperature profiles is shown in figure 10. In this case the T_e profiles are measured at two different times for the same pulse, in a high density H-mode plasma (73340: q_{95}=3.6, 2.7 T/2.5 MA, $n_{e0} = 8 \times 10^{19}$ m^{-3}, $\sim$80$\%$ of the Greenwald density). The profiles in figure 10(a) and (c) have been taken at the beginning and close to the end of the heating phase. The *mtanh* fit to the temperature and density profiles measured by the HRTS for these two time intervals are shown in figure 10(b). It can be seen that an increase in the core density of $\sim$10$\%$, which is the main difference between these two cases, causes an apparent reduction on

the T_e measured in the region ρ <0.85 on the HFS, whereas the pedestal T_e profiles measured at the LFS using 2X-mode ECE are virtually unaffected. An obvious explanation lies in the growing impact of the refraction on the ECE measurements with the increasing density. Since the 1O-mode emission is closer to its cut-off frequency and the distance from the emission location to the antenna is larger, the refraction has a stronger impact on the HFS measurements. Refraction affects the spatial resolution by widening the beam width, but also has a strong influence on the localization of the emission. When the cyclotron resonant frequency is close to its cut-off frequency, plasma refraction significantly affects the wave propagation, causing the ray trajectory to bend away from the horizontal antenna axis. This causes the actual emission location to move outwards so that ρ_{cold} is not longer a valid representation of the position at which the emission is originated[23]. In these conditions, the shift between the mean emission radius and the cold resonance location is significant and must be considered for a correct interpretation of the data. Figure 10(d) shows how the consistency between the LFS and HFS profiles inside the pedestal improves as a result of such analysis, but the difference in the pedestal gradient region remains. It should be mentioned that this calculation is governed not only by the absolute value of the density but also by the details on the density profile and, as a result, and depending on the accuracy of the density profile measurements, a small error in the calculated position may arise.

6. CONCLUSIONS

In this article we have presented the analysis of the first inboard and outboard pedestal temperature profiles measured by the ECE radiometer in JET in a variety of plasma conditions. For a sub-set of magnetic field values, the radiometer allows simultaneous measurements of the HFS (1O-mode, not affected by harmonic overlap) and the LFS (2X-mode) pedestal region with good spatial and temporal resolution. A comprehensive assessment of the quality of such measurements has been carried out using the emission code SPECE. The simulations have shown that the size of the receiving beam is the main contribution to the spatial resolution of 1O-mode emission measurements for frequencies resonating on the HFS midplane. This effect reduces the usefulness of the measurements in the core region, however in the pedestal region, the spatial resolution becomes reasonably small, being the difference between the 1O-mode (HFS) and 2X-mode (LFS) spatial resolutions, ΔR_{95}(1O, HFS)$\sim$2$\times\Delta R_{95}$(2X, LFS) compensated by the difference in flux expansion in the inboard and outboard midplane regions.

Our analysis have demonstrated the usefulness of the 1O-mode ECE measurements to characterize the pedestal T_e profile on the HFS midplane in low to moderate density plasmas. Good agreement, in both shape and magnitude, has been found between the temperature pedestal profiles measured on the HFS (1O-mode ECE) and the LFS (HRTS and 2X-mode ECE). This comparison is only valid for ρ <0.98. Outside this region the optical thickness is significantly reduced (due to the

low n_e and T_e) and the ECE radiation temperature can no longer be interpreted as the local T_e. The main limitation associated with the first harmonic O-mode measurements, in the frequency range explored so far, is related to the growing impact of refraction effects for increasing density. However, this effect is easily alleviated when operating at higher magnetic fields. As a practical criterion, suggested by the experimental results, for reliable 1O-mode ECE measurements on the HFS the plasma density should not be higher than 3/4 of the cut-off density for the corresponding frequency. One of the remaining uncertainties in the analysis of the pedestal profiles from ECE measurements is the uncertainty in the magnetic field calibration and the EFIT equilibrium reconstruction. Despite these uncertainties, the consistency between the HFS and LFS pedestal T_e profiles in the region around and inside the pedestal top is good (within 5-10$\%$), specially considering that these two set of measurements are totally independent (HRTS and 2X-mode ECE in the LFS and 1O-mode in the HFS). This accuracy should be considered acceptable, even though it is clear that the lack of reliable information on the radial profile as measured by ECE in the region near the separatrix leads to large uncertainties in the determination of the temperature pedestal width.

In the work presented here we have focused in the analysis of the spatial features of the measured T_e profiles using the ECE radiometer, being our main concern the validation of the new inboard profile data. Future work will include a more detailed investigation of the fast pedestal dynamics. The high temporal resolution of the existing radiometer in JET together with its capability of obtaining reliable and simultaneous measurements of the T_e pedestal profile on the LFS and the HFS offers the unique opportunity to provide poloidally resolved information on the temporal evolution of the pedestal profiles. Such information is not easily obtained by any other means and therefore it can provide very useful insights into pedestal stability, in particular on the origin of the ELM instability, or perturbative experiments like pellet injection. In addition, HFS T_e measurements can also be very valuable for improving plasma magnetic equilibrium reconstruction. Detailed analysis of these phenomena will be discussed in next publications.

ACKNOWLEDGMENT

This work, supported by the European Communities under the contract of Association between EURATOM/CIEMAT, was carried out within the framework of the European Fusion Development Agreement. The views and opinions expressed herein do not necessarily reflect those of the European Commission.

REFERENCES

[1] Loarte, A., Saibene, G., Sartori, R., et al., Plasma Physics and Controlled Fusion **45** (2003) 1549.

[2] Doyle, E., Houlberg, W., Kamada, Y., et al., Nuclear Fusion **47** (2007) S18.

[3] Nunes, I., Conway, G., Loarte, A., et al., Nuclear Fusion **44** (2004) 883.

[4] Kirk, A., Counsell, G. F., Arends, E., et al., Plasma Physics and Controlled Fusion **46** (2004) A187.

[5] Pasqualotto, R., Nielsen, P., Gowers, C., et al., Review of Scientific Instruments **75** (2004) 3891.

[6] de la Luna, E., Sánchez, J., Tribaldos, V., et al., Review of Scientific Instruments **75** (2004) 3831.

[7] Gowers, C. W., Brown, B. W., Fajemirokun, H., et al., Recent developments in LIDAR Thomson scattering measurements on JET (invited), volume 66, pp. 471–475, AIP, 1995.

[8] O'Brien, D., Lao, L., Solano, E., et al., Nuclear Fusion **32** (1992) 1351.

[9] Farina, D., Figini, L., Platania, P., and Sozzi, C., SPECE: a code for Electron Cyclotron Emission in tokamaks, volume 988, pp. 128–131, AIP, 2008.

[10] Brix, M., Beurskens, M., Boboc, A., and Kempenaars, M., (2009), Submited for publication.

[11] Groebner, R. J. and Carlstrom, T. N., Plasma Physics and Controlled Fusion **40** (1998) 673.

[12] Bartlett, D. V., Physics issues of ECE and ECA for ITER, in *Proc. of the International Workshop on Diagnosic for ITER, 28th August- 1st September 1995 Varenna, Italy*, AIP, 1995.

[13] Buratti, P., Alper, B., Barrera, L., et al., MHD modes localisation in the JET tokamak, in *Proceedings of the 36th EPS Conf. on Plasma Phys.*, 2009.

[14] de la Luna, E., Krivenski, V., Giruzzi, G., et al., Impact of bulk non-Maxwellian electrons on electron temperature measurements (invited), volume 74, pp. 1414–1420, AIP, 2003.

[15] Peeters, A. and Suttrop, W., Physics aspects of the ITER ECE system design, in *Proc. of the 9th Workshop on ECE and ECRH*, 1997.

[16] de la Luna, E., Physics of ECE Temperature Measurements and Prospects for ITER, volume 988, pp. 63–72, AIP, 2008.

[17] Tribaldos, V., EFDA-JET-RE (00)02 Technical report (2001).

[18] Beurskens, M. N. A., Osborne, T. H., Horton, L. D., et al., Plasma Physics and Controlled Fusion **51** (2009) 124051 (15pp).

[19] Solano, E. R., Lomas, P. J., Alper, B., et al., High temperature pedestals in JET and confined current filaments, in *Proceedings of the 36th EPS Conf. on Plasma Phys.*, 2009.

[20] Wolfrum, E., Fischer, R., Langer, B., et al., Pedestal Studies at ASDEX Upgrade, in *Conf. Proc. IAEA 2008*, Geneva, Switzerland, 2008.

[21] Groebner, R., Leonard, A., Snyder, P., et al., Nuclear Fusion **49** (2009) 085037 (14pp).

[22] Giovannozzi, E., Beurskens, M., Boboc, A., et al., Optimizing Performance of Hybrid and AT Dircharges in Preparation for the ITER Like Wall, in *Proceedings of the 36th EPS Conf. on Plasma Phys.*, 2009.

[23] Barrera, L., de la Luna, E., and Figini, L., Comparison of Inboard-Outboard Pedestal Temperature Measurements in JET using ECE Diagnostics, volume 988, pp. 123–127, AIP, 2008.

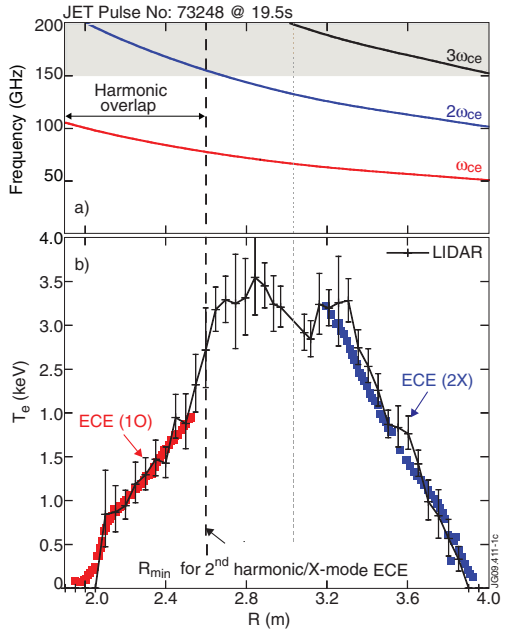

Figure 1: (a) Fundamental, second and third harmonic electron cyclotron frequency along the midplane for JET pulse 73248 (B=2.4 T, I_p=2.0 MA, P_{NBI}=7MW). The frequency region where the second harmonic overlaps with the third harmonic is marked by the shaded area. (b) T_e profile measured by LIDAR and ECE: 2X-mode and 1O-mode ECE are used for access to the LFS and the HFS regions, respectively.

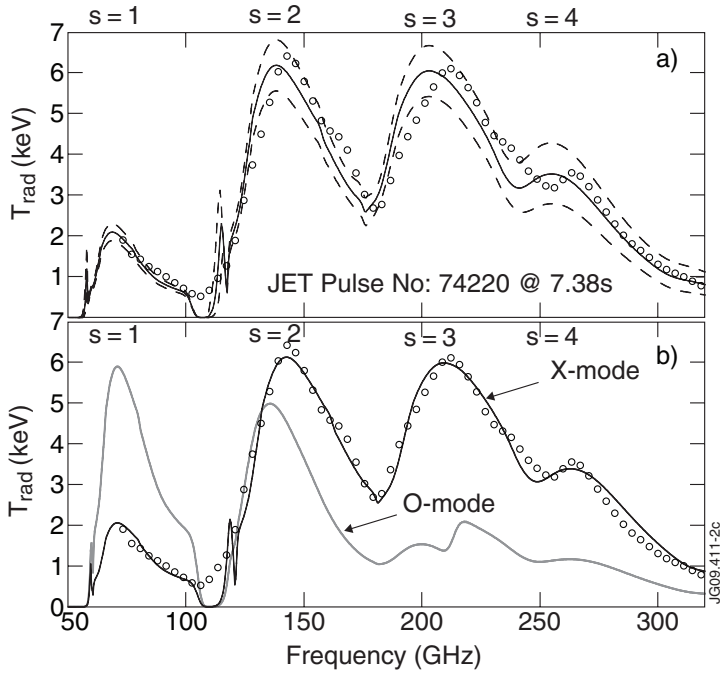

Figure 2: a) Comparison of the measured (open symbols) and simulated (full line) ECE spectrum (quasi X-mode, Michelson interferometer) for a high density H-mode JET pulse (74220, B_0=2.7 T, I_p=1.8 MA). Dashed lines correspond to the spectra obtained including the typical uncertainties ($\sim 10\%$) in the input density and temperature profiles. b) Comparison of the measured (open symbols) and simulated ECE spectrum (black: quasi X-mode and grey: quasi O-mode) assuming a magnetic field calibration error of 3%.

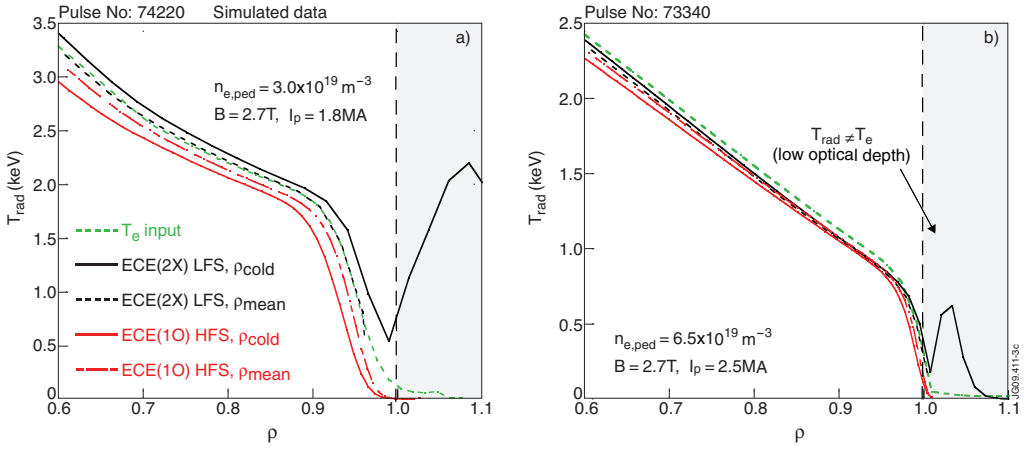

Figure 3: Comparison of the pedestal temperature profiles derived from the 2X-mode (LFS) and the 1O-mode (HFS) ECE simulated spectra to the profile which was used as input for the simulation for two JET pulses with different pedestal plasma parameters: (a) pulse 74220 with $n_{e,ped}$ = 3×10^{19} m^{-3} and $T_{e,ped}$ = 2 keV and (b) pulse 73340 with higher density $n_{e,ped}$ = 6.5×10^{19} m^{-3} and lower temperature $T_{e,ped}$ = 0.8 keV. Both the cold resonance position (full lines) and the mean emission location (dashed lines) are shown. A magnetic field correction of 0.8% was used to match the measured HRTS T_e profile)

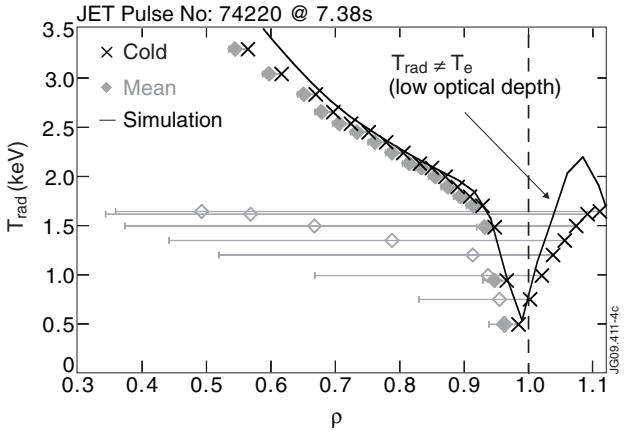

Figure 4: T_e pedestal profile measured by the ECE radiometer (2X-mode) mapped onto the midplane using the cold resonance position of the emitting frequency (black crosses) or the mean emission location (grey symbols) calculated by the SPECE code. In both cases a magnetic field correction factor of 0.8% has been used. Horizontal lines represent the region contributing to the emission. Open symbols correspond to data with low optical thickness for which $T_{rad} \neq T_e$.

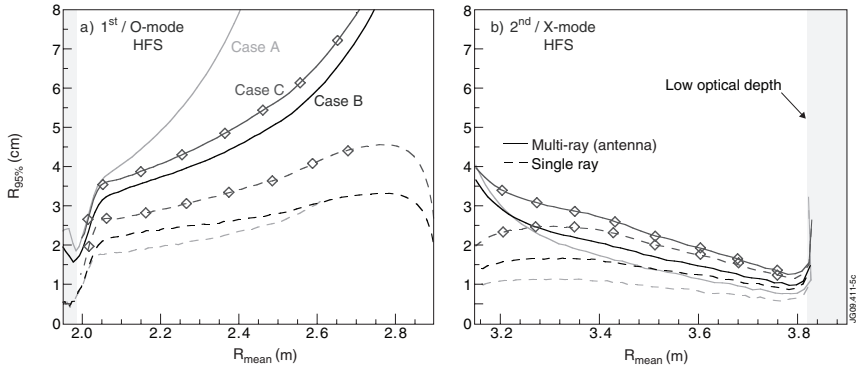

Figure 5: Intrinsic spatial resolution for (a) the 1O-mode ECE and (b) the 2X-mode ECE for a frequency range resonating on the HFS and the LFS respectively. Calculations have been carried out for the JET pulse 73340 (B=2.7 T, I_p=2.5 MA), with $T_{e,ped}$ 1 keV considering different density profiles. Single ray (dash lines) and multi-ray calculations (full line) are shown in the figure.

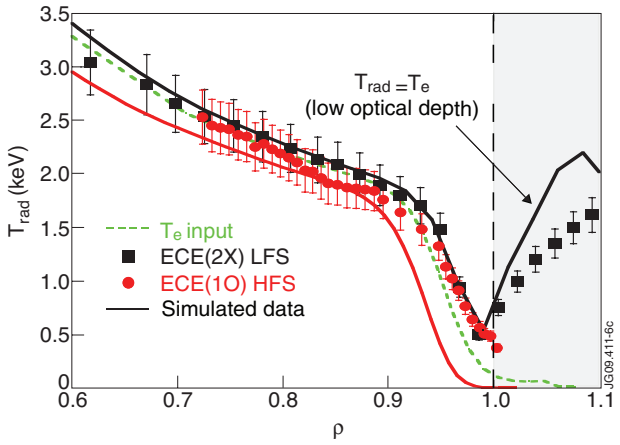

Figure 6: ECE measured (symbols) and calculated (lines) profiles for the JET pulse shown in figure 3. The cold resonance position is used to derive the profiles. The input profile used in the simulation is also shown.

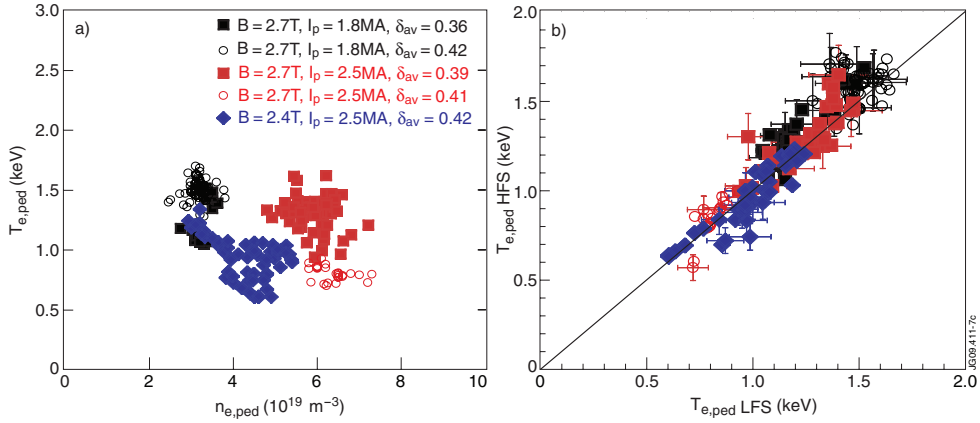

Figure 7: (a) Pedestal T_e and n_e diagram for the pulses used in this analysis showing the different plasma scenarios. (b) Comparison between the pedestal top electron temperature derived from a modified tanh fit of the T_e profiles measured by the ECE radiometer in the LFS (2X-mode) and the HFS (1O-mode) for the dataset shown in (a).

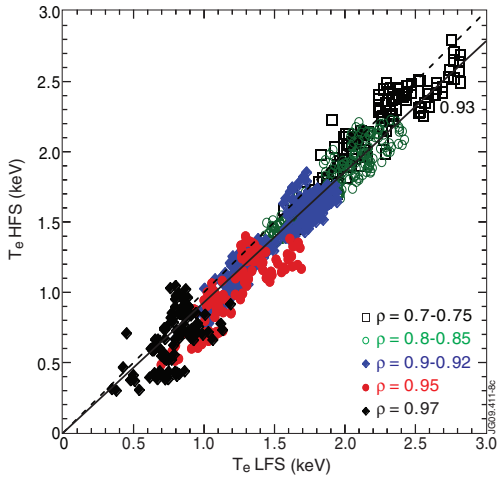

Figure 8: Comparison of the T_e values measured by ECE at the LFS and HFS pedestal region at different radial locations for the dataset shown in figure 7(a)

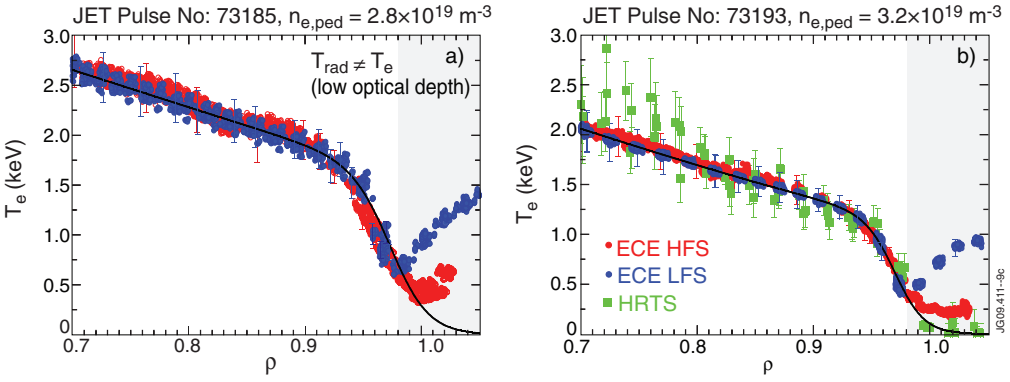

Figure 9: T_e profiles measured by ECE (on the LFS and the HFS) and the HRTS for two JET pulses (AT scenario) with two levels of gas fuelling: a)unfuelled, (b) $10^{21}s^{-1}$. The mtanh fit to the LFS temperature profile data is also shown. The ECE data within the shaded region are excluded from the fit ($T_{rad} \neq T_e$ due to the low optical depth).

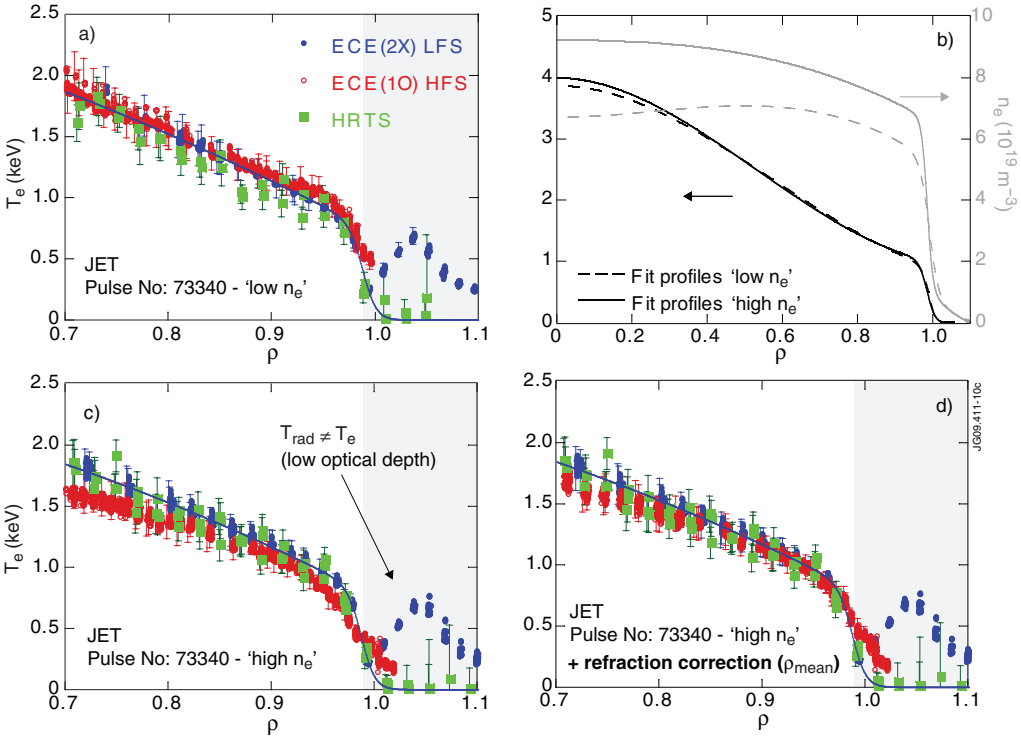

Figure 10: (b) Temperature and density profiles measured by the HRTS for two different time intervals of the JET pulse 73340, (a)-(c) T_e profiles mapped onto the outer midplane measured by the ECE radiometer, both at the LFS (2X-mode) and the HFS (1O-mode) for the two cases shown in (b): 'low' and 'high' density and (d) ECE(1O-mode) profile mapped using the location of the mean emission that takes into account the enhanced refraction effects in the case of higher density. The profiles measured by the HRTS and the results of the mtanh fits for the LFS data (ECE/2X-mode and HRTS) are also shown in the figure (the data with low optical depth, located within the shaded area in the figures, is not included in the fit).